IEEE Access
Multidisciplinary | Rapid Review | Open Access Journal

Received 20 May 2024, accepted 8 July 2024, date of publication 15 July 2024, date of current version 23 July 2024.

Digital Object Identifier 10.1109/ACCESS.2024.3427643

RESEARCH ARTICLE

Estimating of IGBT Bond Wire Lift-Off Trend Using Convolutional Neural Network (CNN)

THATREE MAMEE[1], ZAIQI LOU[1], (Graduate Student Member, IEEE), KATSUHIRO HATA[2], (Member, IEEE), MAKOTO TAKAMIYA[2], (Senior Member, IEEE), TAKAYASU SAKURAI[2], (Life Fellow, IEEE), SHIN-ICHI NISHIZAWA[3], (Member, IEEE), AND WATARU SAITO[3], (Senior Member, IEEE)

[1]Interdisciplinary Graduate School of Engineering Science, Kyushu University, Fukuoka 816-8580, Japan
[2]Institute of Industrial Science, The University of Tokyo, Tokyo 113-8654, Japan
[3]Research Institute for Applied Mechanics, Kyushu University, Fukuoka 816-8580, Japan

Corresponding author: Thatree Mamee (thatree.mam@riam.kyushu-u.ac.jp)

This work was supported in part by the New Energy and Industrial Technology Development Organization (NEDO) under Grant JPNP21009.

ABSTRACT The health monitoring prediction of power devices is vital for power electronics applications such as renewable converters, electric vehicles, and machine drives. One significant failure mode in the power cycle degradation of Insulated Gate Bipolar Transistor (IGBT) modules is bond wire lift-off. This study uses the gate voltage waveform (V_{ge}) as an input to an artificial intelligence (AI) model with the Convolutional Neural Network (CNN). The CNN was demonstrated to accurately estimate the IGBT bond wire lift-off, categorizing it into four levels: no damage, light damage, medium damage, and heavy damage. The Digital Gate Driver (DGD) IC was implemented to generate the V_{ge} and collect the data waveforms by two switching modes: Conventional Vector Control (CVC) and 2-step Vector Control (2-sVC). The experiment evaluated the accuracy of the four-level estimation in several aspects. These aspects include switching modes, the number of datasets, and parts of the waveform The results show that the CNN model achieved high accuracy in estimating the wire lift-off trend. The V_{ge} waveform generated by the 2-sVC switching mode showed better estimation accuracy compared to the CVC mode. Furthermore, it also obtained an effective switching performance E_{loss}-$V_{ce-surge}$ Trade-off curve. Therefore, the DGD is suitable for application and useful for health monitoring and achieving effective switching performance.

INDEX TERMS IGBT power module, health monitoring, power cycle degradation, bond wire.

I. INTRODUCTION

Power cycling degradation of power electronic devices is an important problem for highly reliable power electronic systems such as renewable energy transmission lines, electric vehicles, machine driving, and many other applications [1]. Insulated Gate Bipolar Transistors (IGBTs) are wildly used in power electronic converters, making the IGBT module a necessary component for the reliability of power electronic converters. There are many reasons for IGBT degradation and failure, including thermal cycling, mechanical factors, and material factors [2], [3], [4]. Bond wire lift-off on the IGBT module is a major failure caused by mechanical factors. Aging monitoring has been proposed for investigating IGBT based on the relationship between monitoring parameters and the IGBT aging waveform, serving as a real-time indicator of aging condition [5], [6], [7].

The detection of IGBT bond wires have been proposed using many methods which can be classified into three types: current-based methods, voltage-based methods, and other signal-based methods [16]. First, current-based [17], [18] have shown that short-circuit current is sensitivity to bond wire failures; however, this method requires complex driver circuit and monitoring. Second, voltage-based methods are usually used to measure bond wire faults by detecting increased on-state V_{ce} caused by bond wire lift-off. However, this method has low sensitivity and requires a complex circuit for measurement. The third includes other signal-based

The associate editor coordinating the review of this manuscript and approving it for publication was Zhehan Yi.

methods such as resistance, gate Miller platform duration time, etc. [4], [5], [20]. However, these methods still have low sensitivity for detecting bond wire faults [16].

The parasitic emitter inductance L_{eE} is a phenomenon that increases in value due to bond wire lift-off [8] and is affected by switching waveform, which can be used to indicate degradation caused by bond wire lift-off. Online monitoring using the gate waveform V_{ge} with the Digital Gate Control (DGC) influences the parasitic inductance parameter of the IGBT module. The monitoring method was discussed and proposed for detecting the number of bond wire lift-off [9], [10]. The results show that the V_{ge} waveform can serve as an indicator of the number of wire lift-offs and degradation during online switching operations. Therefore, it is very safe and easy to design the measurement operation.

In the previous work, the bond wire lift-off detection based on turn-on gate voltage was proposed [16]. The result shows that changes in parasitic inductance reflect wire bond lift-off with the turn-on gate voltage overshoot. In contrast, the sensitivity of wire lift-off detection can be expressed by features such as voltage spike peak ($V_{ge\_spike\_peak}$), gate voltage spike amplitude (ΔV_{ge}), and timing shift (Δt_{wire}) as demonstrated in our previous works [9], [10]. Notably, the turn-off waveform exhibits higher $V_{ge\_spike\_peak}$ and ΔV_{ge} compared with turn-on waveform, as shown in an experiment results [22]. Therefore, the turn-off waveform was chosen for detecting by these features.

Many experiments have applied machine learning to estimate degradation and failures in power devices. A feed-forward neural network (FFNN) was used for the prognosis of power MOSFET resistance degradation trend, achieving a correction accuracy was 84.13% [26]. The emitter resistance (R_E) is a key parameter that determines the degradation estimation in power devices. Refs. [12] and [27] proposed R_E estimation by using CNN model with V_{ge} turn-on waveform as the input signal, achieving an accuracy rate of 99.5%. Estimation of reliable remaining useful lifetime (RUL) using parameters V_{ce-on} and a thermal circuit with long short-term memory (LSTM) network models attained maximum accuracies of 97.5% [28] and 97.7% [29], respectively. Deep Neural Networks (DNNs) achieved an accuracy of 96.2% [29], while Random Forest (RF) achieved 96.95% accuracy [29].

This work focuses on V_{ge} turn-off waveform to utilize the phenomena of parasitic inductance to induce voltage influence on gate voltage V_{ge}, including sensitivity features [9], [10] corresponding to voltage overshoot in the turn-off process. Especially, V_{ge} offers advantages such as a simple measurement circuit and safety with low voltage compared with other methods. Additionally, the CNN model has a significant impact on V_{ge} waveform learning, achieving a very high prediction accuracy rate as shown in [12] and [27].

Furthermore, we present the estimated trends in the number of bond wire lift-off by utilizing AI technology to categorize V_{ge} waveforms. Convolutional Neural Network (CNN-based algorithms) was chosen due to its highly efficient image processing capability, high accuracy rates [11], and applicability for learning waveforms to estimate the degradation of power devices.

In addition, DGC not only obtained the waveform for detection bond wire lift-off but also provided precise control of switching behavior and enhanced the trade-off switching characteristics between collector voltage overshoot ($V_{ce-surge}$) and switching loss E_{loss} [13], [14]. Moreover, this paper reports a comparison between conventional vector control (CVC) and 2-step vector control (2-sVC) to achieve both precise control of IGBT switching performance and accurate detection as discussed in this work.

II. EXPERIMENT SETUP AND MONITORING

A. TEST CIRCUIT

The double pulses testing circuit was set to measure the IGBT switching characteristics as shown in Fig. 1. The testing conditions included $V_{dc} = 300$V, $I_e = 100$A, and inductor of 100 μH, and a capacitor of 3900 μF, with testing conducted at a junction temperature of 25 °C. The DGC was implemented to employ a switching step vector control by 6-bit signal control, which consisted of 63 P-type MOSFETs (PMOSs) and 63 N-type MOSFETs (NMOSs) [13].

The gate waveform V_{ge} is influenced not only by the bonding wire effect, but also by the operation voltage, current [10], and temperature [15]. However, parasitic inductance induces a voltage with a large influence on V_{ge} at the high operation current [10]. Therefore, bond wire lift-off detection with parasitic inductance sensitivity should be conducted at a high current and controlled temperature conditions. In this experiment, the operation conditions were fixed at a room temperature of 25 °C, an operating voltage of V_{dc}300 V and test current of 100 A.

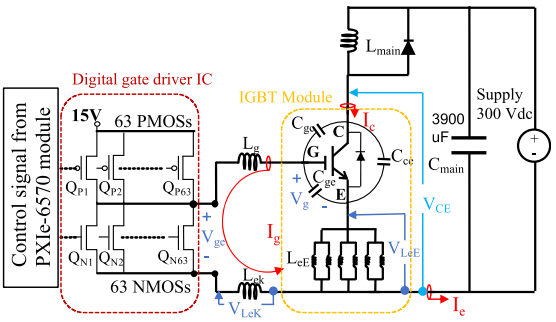

FIGURE 1. Double pulse testing experiment setup and IGBT equivalent circuit.

B. MODULE SETTING FOR MEASUREMENT

The digital gate drive IC can improve the trade-off curve between voltage/current overshoot and switching loss characteristics through step vector control [13]. As a result, digital gate IC can reduce overshoot and switching loss. In this work, we use 2-sVC to improve both trade-offs and increase sensitivity for the reasons mentioned in section III.

This experiment used clock generator supplies a clock signal with a frequency 25MHz to the DGD. A 6-bit input signal is generated by the digital pattern PXIe-6570 module

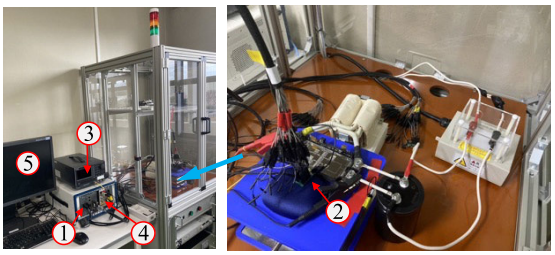

FIGURE 2. Experimental equipment and set-up 1) PXIe-6570 digital pattern 2) Digital Gate Driver IC 3) Clock Generator 4) PXIe-5162 oscilloscope 5) LabView Program.

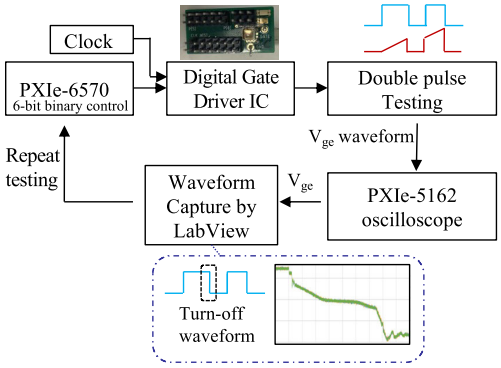

FIGURE 3. V_{ge} turn-off waveform data collection process.

to determine the numbers of vectors within the range of 0 to 63. The waveform was measured by the PXIe-5162 oscilloscope module (Specification: Maximum sample rate of 2.5G/s, bandwidth of 300 MHz (1 MΩ), and bandwidth of 1.5GHz (50 Ω). The experiment setup is shown in Fig. 2.

The LabView program is used to capture waveform data by storing waveform length in memory. The program is configured to command the 6-bit DGC to drive the double pulses, measure the V_{ge} waveforms, and capture turn-off waveform. This process is repeated until the determination round is reached as shown in Fig. 3.

To enable CNN to classify gate voltage waveforms, high-speed sampling is required. In this experiment, a sampling rate of 2.5 GS/s was used. Changes in classification accuracy with respect to the sampling rate need to be examined in the future. Additionally, it is necessary to consider implementing the sampling circuit for gate voltage waveforms, the A/D converter circuit of sampling data, and memory within the gate drive circuit.

The IGBT module ODTMD01250H100 (1250V/100A), made by ODT, was tested in this experiment. The bond wire lift-off was equivalently represented by complete wire lift-off into at four levels of various L_{eE} conditions by cutting 1-3 wires as shown in Fig. 4, corresponding to no damage, light damage, medium damage, and heavy damage. As we repeatedly tested many IGBT modules, we obtained the feature of detection sensitivity, consistent with the result reported in our previous work in [9] and [10]. Therefore, it is applicable for practical use in IGBTs.

Number of wire lift-off representation

- 0 wire-cut is 6 bond wires (No damage)

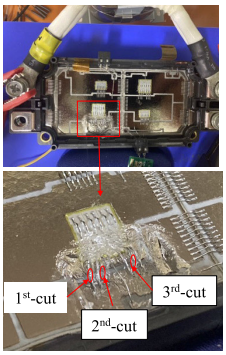

FIGURE 4. IGBT module setup and wire-cut sequence.

- 1 wire-cut is 5 bond wires (Light damage)
- 2 wire-cut is 4 bond wires (Medium damage)
- 3 wire-cut is 3 bond wires (Heavy damage)

III. IGBT TURN-OFF SWITCHING WAVEFORM USING DIGITAL GATE DRIVER

The DGC utilizes a clocked gate driver integrated circuit (IC) to generate an arbitrary gate waveform [13]. DGC was implemented using a programmable gate driver with 63-level drivability, 63 parallel transistors are connected to the gate of IGBT, and a 6-bit control signal is applied to specify the number of activated N_{PMOS} for turn-on and N_{NMOS} for turn-off [14]. This means that the gate current increases with a larger vector number, resulting in increased switching speed and change in switching characteristics V_{ge}, I_g, V_{ce}, and I_e [10]. Two modes of switching were employed to control the turn-off process: (Mode-1) CVC, which involves one-step control with N-level vectors only once, as shown in Fig. 5 (CVC black line); and (Mode-2) 2-sVC, which allows for adjustments in the number of vectors (N_{1st}, N_{2nd}) and duration time (T_{1st}, T_{2nd}) [9], [10], as shown in Fig. 5 (2-sVC red line). N_{1st} operates during the duration time T_{1st}, *and* N_{2nd} operates during the duration time T_{2nd}, allowing for changes in the waveform within a 2-step process. As noted in Refs. [9] and [10], the 2-step control enhances switching performance and wire lift-off detection; therefore, 2-sVC was used in this research.

The characteristics of the turn-off waveform are described in four periods [15] as shown in Fig. 6.

-1st period [t_0-t_1] is the turn-off delay, during which the input capacitor C_{ies} discharges.

-2nd period [t_1-t_2] is the Miller term.

-3rd period [t_2-t_3] sees a rapid increase in V_{ce}, with C_{gc} and C_{ce} drastically decreasing.

-4th period [t_3-t_3] involves V_{ce} rising to the DC bus voltage, followed by a rapid decrease in emitter current I_e, which induces the voltage V_{LeE} and V_{Lek}.

The parasitic emitter inductance L_{eE} performs in the V_{LeE} during the th period due to rapid decrease in I_e. The V_{ge} spike increases as a result of the presence of a large L_{eE}, as given by Eq. (1).

$$V_{ge} = V_g - L_g \frac{di_g}{dt} + L_{ek} \frac{di_g}{dt} - L_{eE} \frac{di_e}{dt} \quad (1)$$

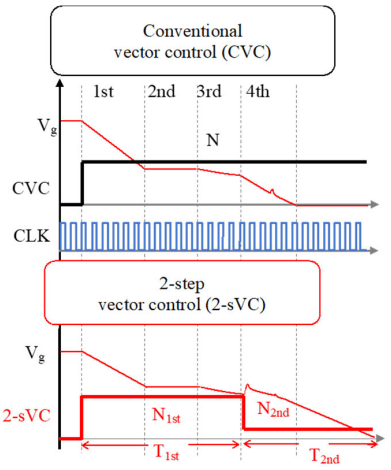

FIGURE 5. The DGC turn-off vectors control pattern.

This experiment proposes two modes of switching control: CVC and 2-sVC, to enhance switching characteristics. CVC is a typical gate driver control method that can change gate current using resistance. However, previous works have found that 2-sVC is useful for enhancing the sensitivity of wire lift-off detection, and the surge voltage ($V_{ce-surge}$) induced by the $L_e \cdot di_e/dt$ (Fig.6) can be suppressed [9], [10]. In 2-sVC, the first vector number (N_{1st}), being large, can reduce switching loss (E_{loss}) that occurs during the transitions between the on-state and off-state. Then, the second vector number (N_{2nd}), being small, is used when the emitter current rapidly decreases to suppress $V_{ce-surge}$ and increase $V_{ge-spike}$, resulting in enhanced sensitivity. Therefore, waveform enhancement, it achieves an effective trade-off between $V_{ce-surge}$ and E_{loss}. Furthermore, the V_{ge} waveform has been improved to enhance sensitivity for high detection accuracy [9], [10].

IV. CONVOLUTIONAL NEURAL NETWORK METHODOLOGY

A. CNN-BASE ARCHITECTURE LAYER

This experiment utilized a deep learning algorithm, Convolutional Neural Network (CNN), to estimate the bond wire lift-off trend, which was categorized into four levels: no damage, light damage, medium damage, and heavy damage, represented by values 0 to 3, respectively. The V_{ge} waveform served as the input dataset, which was obtained through double pulse testing as mentioned in Section II.

The CNN deep learning software is implemented using Python and Keras. The network architecture layer for classifying V_{ge} waveform into four-level categories is shown in Fig. 7. The CNN model uses the following parameter settings:

- Optimizer (iterative optimization algorithm used to minimize the loss function during the training of neural networks) = 'adam' [24]
- Loss (calculated the cross-entropy loss between the true labels and predicted probabilities) = 'sparse_categorical _crossentropy [25]

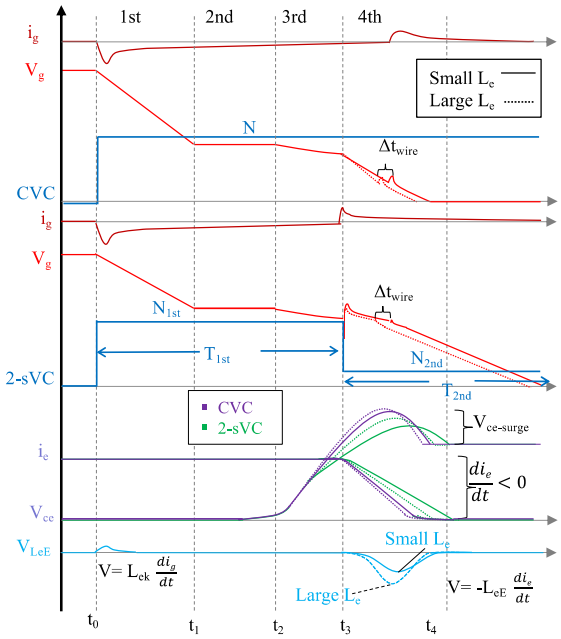

FIGURE 6. Influence of parasitic inductances on turn-off switching.

- Metrics='accuracy' (Percentage of correct prediction) given by Eq. (2).

$$Accuracy = \frac{Number\ of\ Correct\ Predictions}{Total\ Number\ of\ Predictions} \tag{2}$$

Model Derivation: The CNN model consists of the following layers:

1) Reshape Layer: Reshapes the input data for the 1D convolutional layer.
2) Conv1D Layers: Extract features using 1D convolution with ReLU activation.
3) MaxPooling1D Layers: Reduce the dimensionality by taking the maximum value over a window.
4) Flatten Layer: Flattens the input to create a single long feature vector.
5) Dense Layers: Perform the final classification, with the last layer using softmax activation to output probabilities for the four classes.

The parameter coding is shown below:

```
model = keras.Sequential([
    layers.Reshape(target_shape=(length, 1),
input_shape=(length,)),
    layers.Conv1D(32, 3, activation='relu',
input_shape=(length, 1)),
    layers.MaxPooling1D(2),
    layers.Conv1D(64, 3, activation='relu'),
    layers.MaxPooling1D(2),
    layers.Flatten(),
    layers.Dense(128, activation='relu'),
    layers.Dense(4, activation='softmax')
])
```

The training process used batch_size =32, epoch = 40 for all cases to approach the training accuracy at 100%.

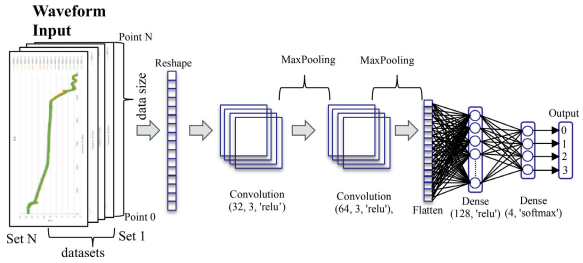

FIGURE 7. Convolutional neural network (CNN) architecture layer.

TABLE 1. DGC vectors control condition.

N vector control	Number of datasets
Conventional control (CVC)	
• $N = 63$	10,000
• $N = 30$	10,000
• $N = 8$	10,000
• $N = 4$	10,000
2-steps vector control (2-sVC)	
• 2-sVC-1 ($N_{1st} = 63$, $T_{1st} = 320$ns, $N_{2nd} = 1$, $T_{2nd} = 4000$ns)	10,000
• 2-sVC-2 ($N_{1st} = 31$, $T_{1st} = 480$ns, $N_{2nd} = 1$, $T_{2nd} = 4000$ns)	10,000
• 2-sVC-3 ($N_{1st} = 21$, $T_{1st} = 720$ns, $N_{2nd} = 1$, $T_{2nd} = 4000$ns)	10,000

B. DATASETS AND WAVEFORM SELECTION

This experiment collected data with 2500 datasets for each level (four levels bond wire lift-off) and under DGC vector control conditions. Thus, the data collection resulted in $4 \times 2500 = 10{,}000$ datasets for each vector control condition as shown in Table 1. The selected conditions were determined based on the E_{loss}-$V_{ce-surge}$ trade-off.

In the CVC condition, the number of vector N was varied to cover a trade-off range from the minimum to maximum V_{surge} level. This range included small vector ($N = 4$), medium vector ($N = 8$), and large vector ($N = 30$) and maximum ($N = 63$) vector levels. At the maximum V_{surge} level, $N = 63$ represents the highest level of vector control. However, it was observed that V_{surge} decreased due to the dynamic avalanche (DA) phenomenon [23].

Typically, turn-off switching behavior is the relationship of E_{loss} decrease with increased V_{surge}. Thus, 2-sVC needs to improve this trade-off by suppressing V_{surge} and decreasing E_{loss} compared to CVC. Therefore, different vector control conditions were considered to achieve minimal E_{loss}, as shown by the dotted red line in Fig. 8, while providing various V_{surge} levels. The 2-sVC-3 condition begins at the minimum V_{surge} level because below this point, V_{surge} is suppressed to a very small level, resulting in minimal sensitivity for wire lift-off detection [9]. 2-sVC-2 was chosen for the highest V_{surge} level, while 2-sVC-1 exhibited small E_{loss}. In 2-sVC-1, $N_{1st} = 63$ represents the maximum vector level, resulting in the smallest waveform among all 2-sVC conditions.

To evaluate the accuracy of the CNN model in selecting the best input waveform conditions under various DGC conditions, each dataset for each condition was divided into

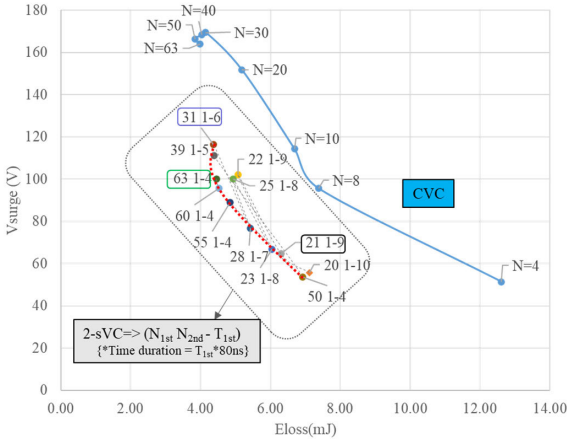

FIGURE 8. E_{loss}-$V_{ce-surge}$ Trade-off curve of CVC and 2-Svc.

training and testing sets. Specifically, 80% of the datasets were allocated for training the CNN model, while the remaining 20% were used for testing the accuracy of the model as shown in Fig. 9. The most significant influence on learning performance depends on the training data, and accurate model evaluation corresponds to the testing data. Therefore, the proportion for splitting data into training and testing datasets was decided to be 80% and 20%, respectively, which is typical practice for ensuring good machine learning performance and accurate model evaluation.

The input data length depends on measurement sampling points used with various vector controls. A varying number of vector controls changes the switching characteristics; for example, when the number of vectors is large, the switching delay time becomes small, and the waveform data points decrease, resulting in a small size of the V_{ge} waveform, as shown in Fig. 10 for CVC and Fig. 11 for 2-sVC. In conclusion, the number of data points can be determined by the number of vector controls (N) with fewer data points observed when the N in large. The V_{ge} waveform generated by CVC at different duration times and spike voltage indicator $\Delta V_{ge-spike}$. Another V_{ge} waveform generated by 2-sVC is shown in Fig. 11, where the switching waveform has been enhanced to increase sensitivity and switching performance as mentioned in [9] and [10].

V. RESULT AND DISCUSSION

The discussion aims to consider the dependences of several aspects to evaluate the accuracy of wire lift-off trend estimation. Thus, this section will be divided into three parts: the aspects of switching control modes, the number of datasets, and the part of waveform that will be significant for achieving high estimation accuracy.

A. ACCURACY OF ESTIMATION DEPENDENCE BY VECTOR CONTROL

The V_{ge} waveform depends on the DGC as mentioned in Section III, with two switching modes: CVC and 2-sVC. The waveform indicator $\Delta V_{ge-spike}$ is affected by bond wire

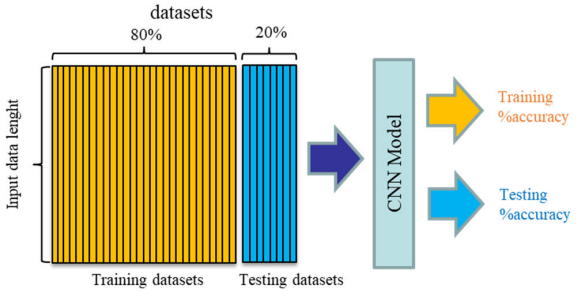

FIGURE 9. Datasets splitting for training and testing CNN model.

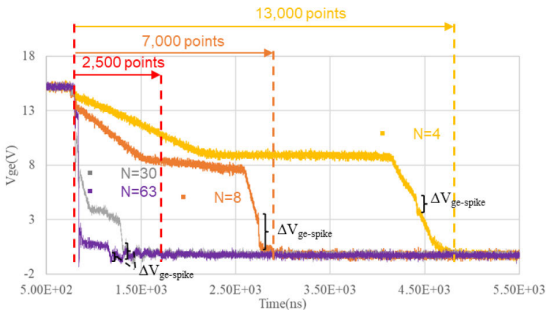

FIGURE 10. Conventional vector control (CVC) waveform input.

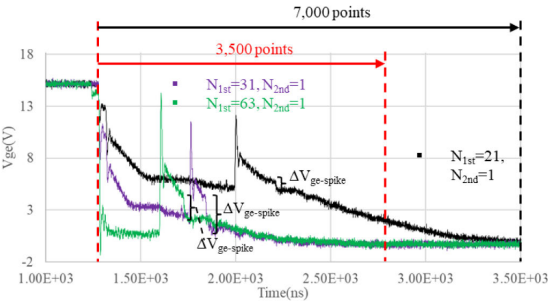

FIGURE 11. 2-steps vector control (2-sVC) waveform input.

lift-off as described in Eq. (1). Therefore, Figure 12 compares the estimation accuracy between dI_e/dt, waveform, and indicator $\Delta V_{ge-spike}$. Since bond wire lift-off affects the waveform indicator differently from dI_e/dt, parasitic inductance induces the gate voltage, as given by Eq. (1). Large dI_e/dt has a greater impact on estimation accuracy of the four-level wire lift-off than $\Delta V_{ge-spike}$, especially when the DA phenomenon occurs, as shown in Fig.12. The maximum accuracy achieved by CVC is 95.25%, and by 2-sVC is 99.60%. As a result, 2-sVC exhibited better accuracy than CVC due to the waveform indicator $\Delta V_{ge-spike}$ by 2-sVC-1 and 2-sVC-2 were larger than CVC $N = 63$ and $N = 30$ respectively.

This experiment used sparse cross-entropy loss [24], which provide output as a probability for classification into value levels and evaluated the output using the accuracy metric as shown in Fig.13. Therefore, CNN output represents the probability of the four-level (0-3) classification of the waveform category as shown in the boxplots in Fig. 14 and Fig. 15. The accuracy of prediction can be assessed by the probability values shown in Figs.14 and Fig.15, which indicate that correct

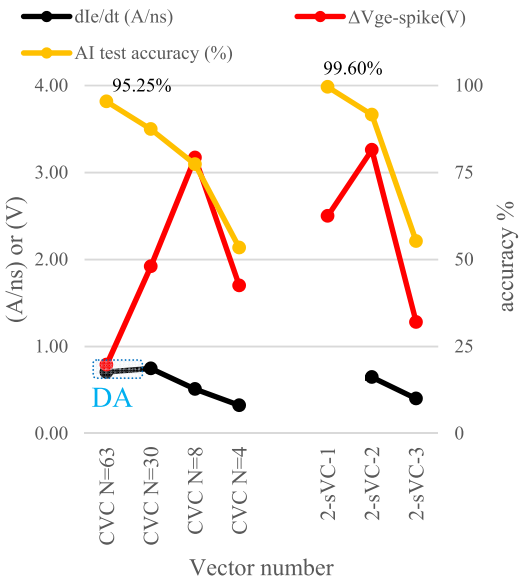

FIGURE 12. CNN accuracy (6wire-3wire) dependence by Vector control.

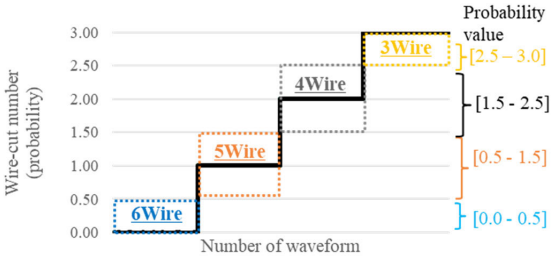

FIGURE 13. CNN accuracy (6wire-3wire) classification probability value.

predictions fall within the square box and incorrect predictions fall outside the square box. Therefore, accuracy can be calculated as the percentage of correct predictions from the entire dataset, as given by Eq. (2). Comparison the input V_{ge} waveform datasets obtained through the two switching modes of vector control, namely CVC with $N = 63$ and 2-sVC-1 with maximum accuracies. The confusion matrix is shown in Figs. 16 and 17, with the F1 score also calculated for each class to evaluate overall accuracy. Comparing the input V_{ge} waveform datasets obtained through the two switching modes of vector control, namely CVC with $N = 63$ and 2-sVC-1 with maximum accuracies of 95.25% (Fig.16) and 99.60% (Fig.17) respectively. The accuracy presented in the confusion matrix can calculate the F1 score to evaluate each class, as shown in Table 2. It was found that the accuracy with 2-sVC-1 is better than CVC for all classes. The results indicate that the input V_{ge} waveform obtained through CVC with $N = 63$ exhibits a greater distribution (outliers) compared to the V_{ge} waveform obtained through 2-sVC. This observation will be further investigated and discussed in Section V Parts C.

B. ACCURACY OF ESTIMATION DEPENDENCE ON THE NUMBER OF DATASETS

The number of datasets is a crucial factor affecting the accuracy and completeness of learning with deep learning CNN

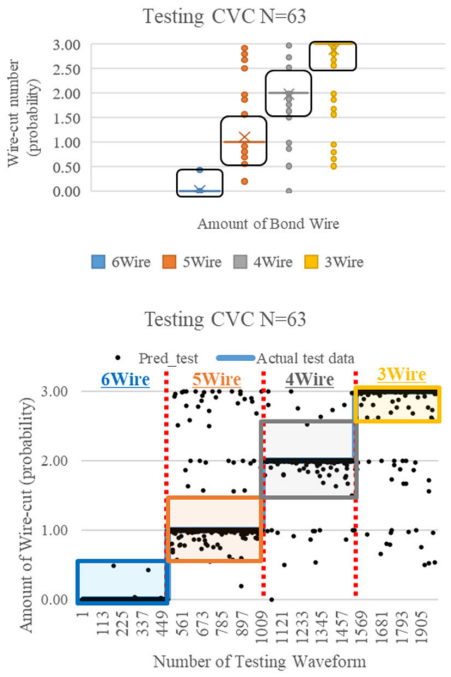

FIGURE 14. CNN testing output probability by CVC N=63 (Accuracy 95.25%).

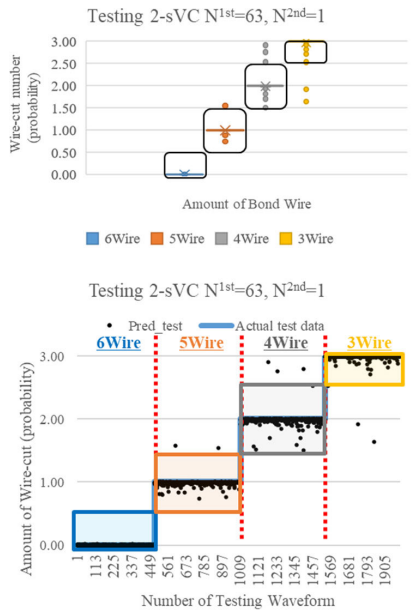

FIGURE 15. CNN testing output probability result by 2-sVC-1 (Accuracy 99.60%).

models. The results show that the V_{ge} waveform obtained through 2-sVC achieved high accuracy with fewer data compared to CVC as shown in Fig. 18. This means that the V_{ge} waveform generated by 2-sVC is highly effective for estimating the trend of bond wire lift-off, owing to its large $\Delta V_{ge-spike}$ and large dI_e/dt as mentioned before.

C. WAVEFORM PART SENSITIVITY FOR DETECTION

This section investigated the significance of sensitivity for wire lift-off detection by analyzing separate V_{ge} waveforms

		Target class				
		6Wire	5Wire	4Wire	3Wire	
Predict class	6Wire	481	1	1	0	99.59%
	5Wire	0	491	13	13	94.97%
	4Wire	0	14	499	16	94.33%
	3Wire	0	27	10	434	92.14%
		100.00%	92.12%	95.41%	93.74%	95.25%

FIGURE 16. Confusion matrix of CVC N=63.

		Target class				
		6Wire	5Wire	4Wire	3Wire	
Predict class	6Wire	481	0	0	0	100.00%
	5Wire	0	531	0	0	100.00%
	4Wire	0	2	519	2	99.24%
	3Wire	0	0	4	461	99.14%
		100.00%	99.62%	99.24%	99.57%	99.60%

FIGURE 17. Confusion matrix of 2-sVC-1.

TABLE 2. F1 score calculation result.

N vector control	F1 score
CVC N=63	
• *6 Wire*	0.9979
• *5 Wire*	0.9352
• *4 Wire*	0.9487
• *3 Wire*	0.9293
(2-sVC-1)	
• *6 Wire*	1
• *5 Wire*	0.9981
• *4 Wire*	0.9924
• *3 Wire*	0.9935

into four parts. The investigation aimed to understand the influence of wire lift-off on changes in the V_{ge} waveform, which results from parasitic emitter inductance L_{eE}. It was found that the waveform exhibits a significant parasitic inductance effect in waveform parts 1-3, and the accuracy achieved with 2-sVC-1 as seen in Fig. 20, is better than that with CVC $N = 63$ as seen in Fig.19. Especially in part 3, 2-sVC-1 achieved a very high accuracy of 98.45% as shown in Fig. 21. The sensitivity was enhanced by 2-sVC-1 with a larger sensitivity compared to CVC $N = 63$ as shown in Fig.22. This suggests that 2-sVC is a good option for enhancing sensitivity to parasitic inductance.

Moreover, 2-sVC achieved effective switching performance as evidenced by the E_{loss}-$V_{ce-surge}$ trade-off curve in Fig. 8, with small E_{loss} and suppressed $V_{ce-surge}$. Because the $V_{ce-surge}$ is induced by the $L_e \cdot di_e/dt$ as shown in Fig.6, the second vector in 2-sVC was set to small number of 1 to

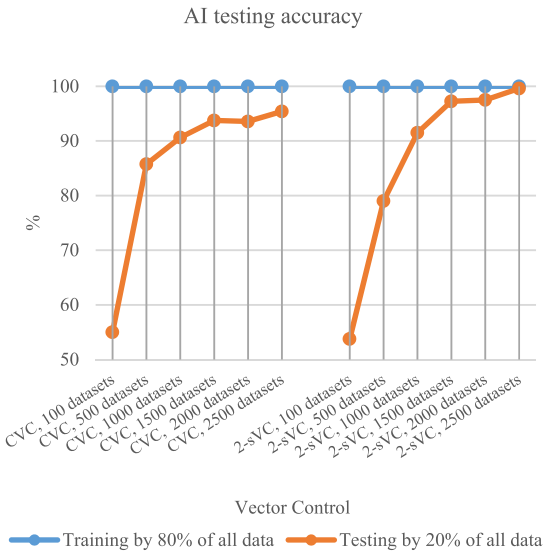

FIGURE 18. CNN accuracy (6wire-3wire) dependence on the number of datasets for each wire lift-off level.

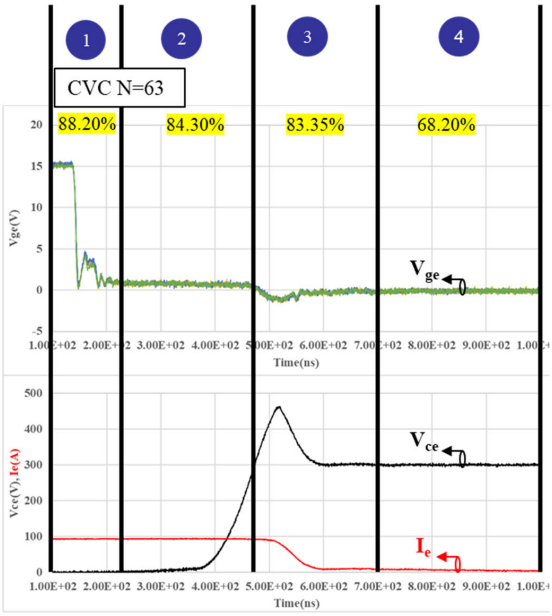

FIGURE 19. Part of waveform sensitivity estimating accuracy (CVC N=63).

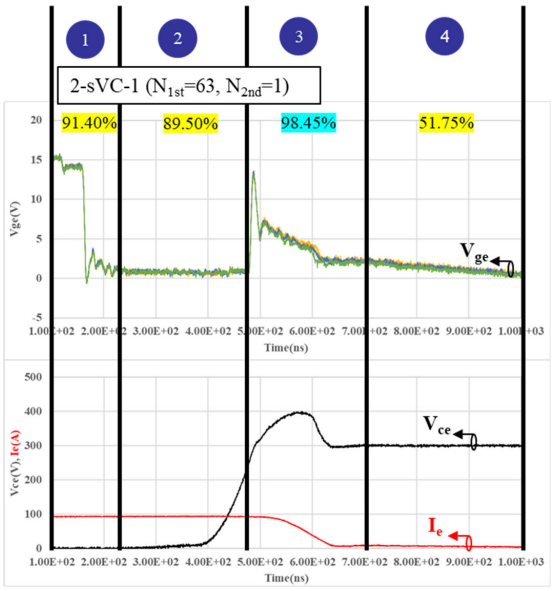

FIGURE 20. Part of waveform sensitivity estimating accuracy (2-sVC-1).

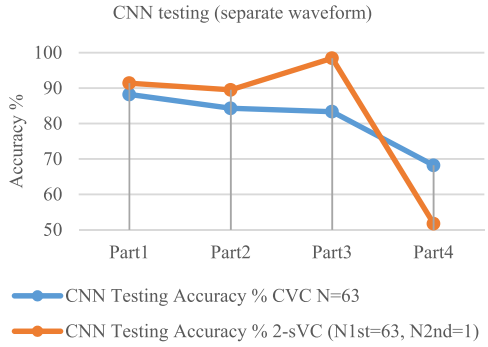

FIGURE 21. Accuracy dependence by waveform part.

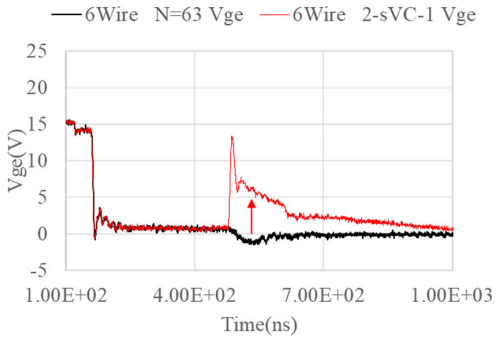

FIGURE 22. Comparison of CVC (N=63) and 2-sVC-1 (N_{1st} = 63, N_{2nd} = 1).

suppress the $V_{ce-surge}$. Although small di_e/dt degrades the detection accuracy in CVC, as shown in Fig. 12, 2-sCV-1 obtained high accuracy even with small die/dt. This is because a large $\Delta V_{ge-spike}$ enhances the sensitivity for wire number. Therefore, 2-sVC can provide both high switching performance and good wire lift-off detection.

The test conditions in this experiment were fixed at room temperature, with an operating current of 100 A and an applied voltage of 300 V. However, in real operation, the switching waveform varies with the operating conditions. Therefore, as future work, detection under various temperatures and diverse operating conditions will be investigated to approach real applications.

VI. CONCLUSION

In this work, we present a deep-learning algorithm based on CNN for estimating the trend of IGBT bond wire lift-off, which is categorized into four levels of damage. V_{ge} waveforms generated by CVC and 2-sVC under various conditions were used as input waveform data for the CNN model to evaluate the best estimation accuracy. The results show that the CNN model achieved good accuracy in estimating the four levels of bond wire lift-off at 95.25% and 99.60% with CVC and 2-sVC input waveform, respectively. Particularly, the 2-sVC condition exhibited better estimation accuracy than

CVC, considering the smaller number of datasets required for training and the sensitivity of waveform detection. Moreover, DGD with 2-sVC achieved not only high accuracy in estimating the trend of IGBT bond wire lift-off but also effective switching performance, as demonstrated by the E_{loss}-$V_{ce-surge}$ trade-off curve.

REFERENCES

[1] S. Yang, A. Bryant, P. Mawby, D. Xiang, L. Ran, and P. Tavner, "An industry-based survey of reliability in power electronic converters," in *Proc. IEEE Energy Convers. Congr. Expo.*, San Jose, CA, USA, Sep. 2009, pp. 3151–3157, doi: 10.1109/ECCE.2009.5316356.

[2] A. Morozumi, K. Yamada, T. Miyasaka, and Y. Seki, "Reliability of power cycling for IGBT power semiconductor modules," in *Proc. Conf. Rec. IEEE Ind. Appl. Conf., 36th IAS Annu. Meeting*, vol. 3, Chicago, IL, USA, Oct. 2001, pp. 1912–1918, doi: 10.1109/IAS.2001.955791.

[3] W. Kexin, D. Mingxing, X. Linlin, and L. Jian, "Study of bonding wire failure effects on external measurable signals of IGBT module," *IEEE Trans. Device Mater. Rel.*, vol. 14, no. 1, pp. 83–89, Mar. 2014, doi: 10.1109/TDMR.2012.2200485.

[4] D. Luo, M. Chen, W. Lai, H. Xia, X. Ding, and Z. Deng, "A study on the effect of bond wires lift-off on IGBT thermal resistance measurement," *Electronics*, vol. 10, no. 2, p. 194, Jan. 2021, doi: 10.3390/electronics10020194.

[5] J. Liu, G. Zhang, Q. Chen, L. Qi, Y. Geng, and J. Wang, "In situ condition monitoring of IGBTs based on the Miller Plateau duration," *IEEE Trans. Power Electron.*, vol. 34, no. 1, pp. 769–782, Jan. 2019, doi: 10.1109/TPEL.2018.2820700.

[6] R. Zheng, H. Xu, C. Li, W. Li, X. He, H. Luo, and D. Li, "Online aging parameter extraction with induced voltage v_{eE} between Kelvin and power emitter in turn-off progress for IGBT modules," in *Proc. IEEE Energy Convers. Congr. Expo. (ECCE)*, Portland, OR, USA, Sep. 2018, pp. 362–366, doi: 10.1109/ECCE.2018.8557554.

[7] Z. Hu, X. Ge, D. Xie, Y. Zhang, B. Yao, J. Dai, and F. Yang, "An aging-degree evaluation method for IGBT bond wire with online multivariate monitoring," *Energies*, vol. 12, no. 20, p. 3962, Oct. 2019, doi: 10.3390/en12203962.

[8] Y. Shen, J. Jiang, Y. Xiong, Y. Deng, X. He, and Z. Zeng, "Parasitic inductance effects on the switching loss measurement of power semiconductor devices," in *Proc. IEEE Int. Symp. Ind. Electron.*, Montreal, QC, Canada, Jul. 2006, pp. 847–852, doi: 10.1109/ISIE.2006.295745.

[9] T. Mamee, Z. Lou, K. Hata, M. Takamiya, S.-I. Nishizawa, and W. Saito, "Enhancement of turn-off gate voltage waveform change by digital gate control for bond wire lift-off detection in IGBT module," *Microelectron. Rel.*, vol. 147, Aug. 2023, Art. no. 115067, doi: 10.1016/j.microrel.2023.115067.

[10] T. Mamee, Z. Lou, K. Hata, M. Takamiya, S.-I. Nishizawa, and W. Saito, "Bond wire lift-off detection by gate voltage waveform in IGBT turn-off process enhanced by digital gate control," *Power Electron. Devices Compon.*, vol. 6, Oct. 2023, Art. no. 100052, doi: 10.1016/j.pedc.2023.100052.

[11] R. M. Shah, B. Sainath, and A. Gupta, "Comparative performance study of CNN-based algorithms and Yolo," in *Proc. IEEE Int. Conf. Electron., Comput. Commun. Technol. (CONECCT)*, Bengaluru, India, Jul. 2022, pp. 1–6, doi: 10.1109/CONECCT55679.2022.9865820.

[12] K. Miyazaki, Y. Lo, A. K. M. Mahfuzul Islam, K. Hata, M. Takamiya, and T. Sakurai, "CNN-based approach for estimating degradation of power devices by gate waveform monitoring," in *Proc. Int. Conf. IC Design Technol. (ICICDT)*, Suzhou, China, Jun. 2019, pp. 1–4, doi: 10.1109/ICICDT.2019.8790833.

[13] K. Miyazaki, S. Abe, M. Tsukuda, I. Omura, K. Wada, M. Takamiya, and T. Sakurai, "General-purpose clocked gate driver IC with programmable 63-level drivability to optimize overshoot and energy loss in switching by a simulated annealing algorithm," *IEEE Trans. Ind. Appl.*, vol. 53, no. 3, pp. 2350–2357, May 2017, doi: 10.1109/TIA.2017.2674601.

[14] T. Sai, K. Miyazaki, H. Obara, T. Mannen, K. Wada, I. Omura, M. Takamiya, and T. Sakurai, "Load current and temperature dependent optimization of active gate driving vectors," in *Proc. IEEE Energy Convers. Congr. Expo. (ECCE)*, Baltimore, MD, USA, Sep. 2019, pp. 3292–3297, doi: 10.1109/ECCE.2019.8913103.

[15] H. Luo, Y. Chen, P. Sun, W. Li, and X. He, "Junction temperature extraction approach with turn-off delay time for high-voltage high-power IGBT modules," *IEEE Trans. Power Electron.*, vol. 31, no. 7, pp. 5122–5132, Jul. 2016, doi: 10.1109/TPEL.2015.2481465.

[16] Y. Yang and P. Zhang, "A novel bond wire fault detection method for IGBT modules based on turn-on gate voltage overshoot," *IEEE Trans. Power Electron.*, vol. 36, no. 7, pp. 7501–7512, Jul. 2021, doi: 10.1109/TPEL.2020.3047135.

[17] P. Sun, C. Gong, X. Du, Y. Peng, B. Wang, and L. Zhou, "Condition monitoring IGBT module bond wires fatigue using short-circuit current identification," *IEEE Trans. Power Electron.*, vol. 32, no. 5, pp. 3777–3786, May 2017, doi: 10.1109/TPEL.2016.2585669.

[18] P. Sun, C. Gong, X. Du, Q. Luo, H. Wang, and L. Zhou, "Online condition monitoring for both IGBT module and DC-link capacitor of power converter based on short-circuit current simultaneously," *IEEE Trans. Ind. Electron.*, vol. 64, no. 5, pp. 3662–3671, May 2017, doi: 10.1109/TIE.2017.2652372.

[19] B. Ji, V. Pickert, W. Cao, and B. Zahawi, "In situ diagnostics and prognostics of wire bonding faults in IGBT modules for electric vehicle drives," *IEEE Trans. Power Electron.*, vol. 28, no. 12, pp. 5568–5577, Dec. 2013.

[20] Mohd. A. Eleffendi and C. M. Johnson, "In-service diagnostics for wire-bond lift-off and solder fatigue of power semiconductor packages," *IEEE Trans. Power Electron.*, vol. 32, no. 9, pp. 7187–7198, Sep. 2017.

[21] S. Beczkowski, P. Ghimre, A. R. de Vega, S. Munk-Nielsen, B. Rannestad, and P. Thøgersen, "Online Vce measurement method for wear-out monitoring of high power IGBT modules," in *Proc. 15th Eur. Conf. Power Electron. Appl. (EPE)*, Lille, France, Sep. 2013, pp. 1–7, doi: 10.1109/EPE.2013.6634390.

[22] Z. Lou, T. Mamee, K. Hata, M. Takamiya, S.-I. Nishizawa, and W. Saito, "IGBT power module design for suppressing gate voltage spike at digital gate control," *IEEE Access*, vol. 11, pp. 6632–6640, 2023, doi: 10.1109/ACCESS.2023.3237266.

[23] P. Luo, S. N. E. Madathil, S.-I. Nishizawa, and W. Saito, "Evaluation of dynamic avalanche performance in 1.2-kV MOS-bipolar devices," *IEEE Trans. Electron Devices*, vol. 67, no. 9, pp. 3691–3697, Sep. 2020, doi: 10.1109/TED.2020.3007594.

[24] *Optimizer That Implements the Adam Algorithm*. Accessed: May 12, 2024. [Online]. Available: https://www.tensorflow.org/api_docs/python/tf/keras/optimizers/Adam

[25] *Computes the Crossentropy Loss Between the Labels and Predictions*. Accessed: May 12, 2024. [Online]. Available: https://www.tensorflow.org/api_docs/python/tf/keras/losses/SparseCategoricalCrossentropy

[26] K. Pugalenthi, H. Park, and N. Raghavan, "Prognosis of power MOSFET resistance degradation trend using artificial neural network approach," *Microelectron. Rel.*, vols. 100–101, Sep. 2019, Art. no. 113467, doi: 10.1016/j.microrel.2019.113467.

[27] H. Yamasaki, K. Miyazaki, Y. Lo, A. K. M. Mahfuzul Islam, K. Hata, T. Sakurai, and M. Takamiya, "Power device degradation estimation by machine learning of gate waveforms," in *Proc. Int. Conf. Simulation Semiconductor Processes Devices (SISPAD)*, Kobe, Japan, Sep. 2020, pp. 335–338, doi: 10.23919/SISPAD49475.2020.9241607.

[28] W. Li, B. Wang, J. Liu, G. Zhang, and J. Wang, "IGBT aging monitoring and remaining lifetime prediction based on long short-term memory (LSTM) networks," *Microelectron. Rel.*, vol. 114, Nov. 2020, Art. no. 113902, doi: 10.1016/j.microrel.2020.113902.

[29] M. Moniruzzaman, A. H. Okilly, S. Choi, J. Baek, T. I. Mannan, and Z. Islam, "A comprehensive study of machine learning algorithms for GPU based real-time monitoring and lifetime prediction of IGBTs," in *Proc. IEEE Appl. Power Electron. Conf. Expo. (APEC)*, Long Beach, CA, USA, Feb. 2024, pp. 2678–2684, doi: 10.1109/apec48139.2024.10509167.

THATREE MAMEE received the M.S. degree in electrical engineering from Kasetsart University, Bangkok, Thailand, in 2012. He is currently pursuing the Ph.D. degree with the Power Electronics Group, Interdisciplinary Graduate School of Engineering Science.

Since 2012, he has been with the Clean Energy Systems Integration Laboratory, King Mongkut's University of Technology Thonburi. His research interests include power electronics and power devices.

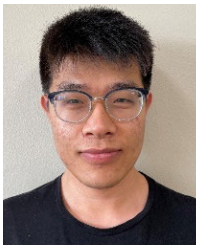

ZAIQI LOU (Graduate Student Member, IEEE) received the M.S. degree from Kyushu University, Fukuoka, Japan, in 2021. He is currently pursuing the Ph.D. degree with the Power Electronics Group, Interdisciplinary Graduate School of Engineering Science.

His research interests include solid-state circuit breakers and power modules.

KATSUHIRO HATA (Member, IEEE) received the Ph.D. degree in electrical engineering from The University of Tokyo, Tokyo, Japan, in 2018. He is currently a Research Associate with the Institute of Industrial Science, The University of Tokyo. His research interests include hybrid dc–dc converters, digital active gate driving, wireless power transfer, and e-mobility for transportation. He was a recipient of the Best Paper Award in 2018 IEEE Transportation Electrification Conference and Expo, the Asia-Pacific (ITEC-AP), and the William M. Portnoy First Prize Paper Award in 2022 IEEE Energy Conversion Congress and Exposition (ECCE).

MAKOTO TAKAMIYA (Senior Member, IEEE) received the B.S., M.S., and Ph.D. degrees in electronic engineering from The University of Tokyo, Tokyo, Japan, in 1995, 1997, and 2000, respectively.

In 2000, he joined NEC Corporation, Tokyo, Japan, where he was engaged in the circuit design of high-speed digital LSIs. In 2005, he joined The University of Tokyo, where he is currently a Professor with the Institute of Industrial Science. From 2013 to 2014, he was with the University of California at Berkeley, Berkeley, CA, USA, as a Visiting Scholar. His research interests include integrated power management circuits for wireless powering and energy harvesting for wearable and IoT applications and digital gate driver IC for power electronics.

Prof. Takamiya is a member of the Technical Program Committee of the IEEE Symposium on VLSI Circuits. He was formerly a member of the Technical Program Committees of the IEEE International Solid-State Circuits Conference (ISSCC), from 2015 to 2020; and the IEEE Custom Integrated Circuits Conference, from 2006 to 2011. He was the Far East Regional Chair in ISSCC 2020. He was a recipient of the 2009 and 2010 IEEE Paul Rappaport Awards and the Best Paper Award of the 2013 IEEE Wireless Power Transfer Conference. He is a Distinguished Lecturer of the IEEE Solid-State Circuits Society.

TAKAYASU SAKURAI (Life Fellow, IEEE) received the Ph.D. degree in EE from The University of Tokyo, in 1981. In 1981, he joined Toshiba Corporation, where he designed CMOS DRAM, SRAM, RISC processors, DSPs, and SoC solutions. He has worked extensively on interconnect delay and capacitance modeling known as Sakurai model and alpha power-law MOS model. From 1988 to 1990, he was a Visiting Researcher with the University of California at Berkeley, where he conducted research in the field of VLSI CAD. Since 1996, he has been a Professor with The University of Tokyo, working on low-power high-speed VLSI design, memory design, organic IC's, low-power IoT systems platform, and power electronics. Currently, he is a Professor Emeritus with The University of Tokyo and the Chairperson of the Trillion-Node Research Group. He has delivered keynote speeches at more than 50 conferences, including ISSCC. He was a domain research supervisor for nano-electronics area with Japan Science and Technology Agency. He is an IEICE Fellow. He was a recipient of many awards, including the IEEE Donald O. Pederson Award in Solid-State Circuits and the IEEE Paul Rappaport Award. He has served as the Executive Chair for IEEE VLSI Symposia and IEEE A-SSCC.

SHIN-ICHI NISHIZAWA (Member, IEEE) received the B.Eng., M.Eng., and Dr.Eng. degrees in chemical engineering from Waseda University, Tokyo, Japan, in 1989, 1991, and 1994, respectively.

Then, he joined Waseda University, as a Research Associate. In 1996, he joined the Electrotechnical Laboratory, Tsukuba, Japan, (since 2001, the National Institute of Advanced Industrial Science and Technology). Since 2017, he has been with Kyushu University, Kasuga, Japan. He has worked on power semiconductor material processes and power devices. His research interests include semiconductor wafer technologies for power devices and power electronics components and systems.

WATARU SAITO (Senior Member, IEEE) received the B.Eng., M.Eng., and Dr.-Eng. degrees in electrical and electronics engineering from Tokyo Institute of Technology, Tokyo, Japan, in 1994, 1996, and 1999, respectively.

Since 1999, he has been with Toshiba Corporation, Kawasaki, Japan, where he engaged in the development of power semiconductor devices. Since 2019, he has been with Kyushu University, Kasuga, Japan. His current research interests include basic research on next-generation power semiconductor devices including related application technologies.

Dr. Saito was a recipient of the Conference Prize Paper Award in 2008 IEEE Power Electronics' Specialists Conference. He formerly served as a Committee Member for Power Devices and ICs Committee, IEEE Electron Device Society, from 2015 to 2020. He is an Editor of IEEE TRANSACTIONS ON ELECTRON DEVICES.